Separation and Purification Technology 306 (2023) 122695

Contents lists available at ScienceDirect

Separation and Purification Technology

journal homepage: www.elsevier.com/locate/seppur

Kinetic process assessment of H_2 purification over highly porous carbon sorbents under multicomponent feed conditions

Khaled Baamran [a], Qasim Al-Naddaf [a], Shane Lawson [a], A. Ali Rownaghi [b], Fateme Rezaei [a,*]

[a] Linda and Bipin Doshi Department of Chemical and Biochemical Engineering, Missouri University of Science and Technology, Rolla, MO 65409-1230, United States
[b] Department of Chemistry, Cleveland State University, Cleveland, OH 44115, United States

ARTICLE INFO

Keywords:
H_2 purification
Activated carbon
Multicomponent adsorption
PSA

ABSTRACT

As a universal energy carrier, the need for pure H_2 is ever increasing due to its ubiquitous role in petrochemical refining, metal reduction, and the up-and-coming fuel cell market. Hydrogen produced from steam methane reforming (SMR) is typically laden with impurities such as CO_2, CO, and CH_4 and a full efficiency screening for potential H_2 purification sorbents requires evaluating the thermodynamic and kinetic behaviors associated with multicomponent pressure swing adsorption (PSA). As such, in this study we assessed three commercially available activated carbons with high surface area and pore volume for the PSA upgrading of H_2 from simulated SMR off-gas stream consisting of $H_2/CO/CH_4/CO_2$ (75/5/5/15 vol%). In addition to high-pressure adsorption isotherms for pure gases, H_2 purity and recovery, and H_2 productivity were estimated from cyclic PSA experiments, while actual $(CO + CH_4 + CO_2)/H_2$ selectivity values were estimated from breakthrough experiments. For the best performing material, the results demonstrated H_2 purity and recovery of 99.6 and 55.3 %, respectively with a productivity of 18.3 $mol_{H2}/kg{\cdot}h$ and multicomponent $(CO + CH_4 + CO_2)/H_2$ selectivity of 59.86 %. Moreover, the affinity of the different adsorbates toward the activated carbons presented from the most adsorbed to the least adsorbed gas was in the order of $CO_2 > CH_4 > CO \gg H_2$. The H_2 purification over these carbon-based adsorbents was found to be an equilibrium-controlled process.

1. Introduction

It is estimated that approximately 120 million tons of H_2 is produced annually for industries such as petrochemical refining, and ammonia or methanol synthesis with production requirements likely to rise in the coming decades due to the foreseeable increase in demand from the H_2 fuel cell automotive sector.[1] Especially in that sector, ultra-high purity (UHP) H_2 is required because a low-purity feedstock – i.e., 99 % instead of 99.999 % H_2 – is known to reduce the electrochemical potential of the fuel cell and can cause anode corrosion over time.[2–5] Therefore, the need for high-purity H_2 is undeniable and can be considered an important aspect of various chemical industries. Nevertheless, as-received H_2 most often comes from natural gas fracturing or other petrochemical industries including steam methane reforming (SMR), which typically contains impurities such as CO_2, CO, and CH_4 that lower the H_2 energy density.[2,6–10] As such, H_2 sources must be upgraded to higher purity for viability in such applications.

In industry, H_2 upgrading is achieved using pressure swing adsorption (PSA) processing,[11–13] whereby the contaminated stream is flown through an adsorbent bed that has been pressurized with the light component of the feed (i.e., H_2), thus ensuring adsorption of the undesirable contaminants and purification of the light species.[14,15] Such PSA processes are standard in industry and they are a well-recognized approach for purifying H_2, with the most commonly used materials being are activated carbon.[1,16–18] The reasons for such common employment of activated carbon for H_2 upgrading are i) its low cost, ii) tunable physiochemical properties, and iii) ability to be synthesized from agricultural waste products that otherwise would not be marketable.[19–21] To date, there have been a myriad of studies which employ activated carbon for PSA upgrading of H_2, such as Lopes et al.[1] who investigated the vacuum PSA (VPSA) performance of activated carbon adsorbents in a ten step system and reported 99.98 % H_2 purity, 81.6 % H_2 recovery, and 101 mol_{H2}/kg_{ads}.day productivity. However, well-established as this area may be in both the academic and industrial sectors, it is worth noting that studies focusing on the separation performance of carbonaceous sorbents for H_2 upgrading often focused on purifying binary feedstocks, whereas as-received H_2 streams typically contain multiple components when generated from petrochemical

* Corresponding author.
E-mail address: rezaeif@mst.edu (F. Rezaei).

https://doi.org/10.1016/j.seppur.2022.122695
Received 18 August 2022; Received in revised form 10 November 2022; Accepted 14 November 2022
Available online 19 November 2022

sources as previously alluded.[1].

These multicomponent feeds generally exhibit competitive or so-called "kick-out" adsorbent behaviors, whereby heavier species displace the lighter species from the pore windows. These effects are especially downstream of SMR processes, since the CO_2, CO, and CH_4 components are of similar molecular sizes but varying weights, meaning that their multicomponent competitive behaviors are more prevalent as opposed to other processes. To date, however, literature focused on understanding these multicomponent interactions, even in commonplace materials such as activated carbon, has been scarce. In particular, the kinetic separation behaviors and thermodynamic properties (i.e., cyclic heat transfer) under multicomponent feed conditions and working multicomponent (i.e., (CO_2 + CO + CH_4)/H_2) selectivities which are consistent with SMR off-gas is an area which has seldomly been studied. Given that such knowledge can eventually be used to drive improvements at the process level since the overall cycle time depends on the choice of adsorbent – especially regarding the sorbent textural properties and multicomponent exclusivity behaviors – it could reasonably be expected that adsorbents with better multi-component efficiency can yield higher H_2 purity without significant compromises in hourly productivity. Hence, understanding these properties which are underdeveloped overall is an important aspect to better optimizing the final PSA performance at the industrial level.

Motivated by the need to further develop the area of H_2 PSA upgrading under multicomponent feed conditions, with particular emphasis on understanding how the transport properties of multiple SMR feed components are influenced by the textural properties of the carbon and how this translates to overall PSA performance, we embarked on a study which investigates the performance of three commercially available activated carbon materials from Ingevity corporation under a mixture of CO_2, CO, CH_4, and H_2. This was accomplished through a combination of high-pressure adsorption isotherms, high-pressure single-breakthrough experiments with simulated SMR feedstocks, and cyclic PSA experiments. The adsorption isotherms revealed that all three carbons were highly selective towards CO, CO_2, and CH_4 relative to H_2 – especially at elevated pressure – but had varying degrees of CO_2/CH_4, CO_2/CO, and CO/CH_4 selectivities which could yield multicomponent adsorption interactions. Indeed, the single-breakthrough experiments confirmed these effects, as all samples showed significant losses in single-component adsorption capacity compared to the expected values from the adsorption isotherms when a multicomponent SMR mixture was used. From the PSA experiments, it was revealed that high H_2 purity with reasonably high productivity can be achieved over these highly porous materials, albeit with a relatively low recovery compared to the current benchmark adsorbents.

2. Experimental section

2.1. Characterization of sorbents

Three commercially available activated carbon samples, namely AC-3 (crushed 1.55 mm), AC-6 (beads 2.25 mm), and AC-9 (beads 2.75 mm) were used as-received from Ingevity Inc. The textural properties of the materials were assessed via N_2 physisorption at 77 K on a Micromeritics (3Flex) gas analyzer. The surface area and pore distributions of the materials were calculated from the physisorption data using the Braunner-Emmett-Teller (BET) and nonlocal density functional theory (NLDFT) methods, respectively. Prior to analysis, the samples were evacuated at 350 °C for 6 h on a Micromeritics SmartVac Prep system. The skeletal density (ρ_{ske}) of the sample was estimated from helium adsorption at 25 °C on BELSORP-HP instrument. Before these measurements, the adsorbent was degassed at 350 °C under vacuum for 6 h, while bulk density (ρ_{bulk}) was evaluated through helium pycnometry on a Micromeritics AccuPyc II 1340 instrument by loading the sample into a cylindrical steel mold and applying a mechanical pressure of 500 bar.

2.2. Adsorption isotherm measurements

High-pressure adsorption-desorption isotherms of CO_2, CH_4, H_2, and CO were collected at 25 °C over a pressure range of 0–50 bar on a BELSORP HP gas analyzer. All samples were degassed at 350 °C for 6 h prior to the analysis. The total adsorption capacities were determined from the excess volumetric data measured by the instrument using **Eq. (1)**:

$$q_{tot}(P,T) = \frac{q_{exc}(P,T)}{\left(1 - \frac{\rho_{gas}(P,T)}{\rho_{sat}}\right)} \quad (1)$$

where q_{exc} (P,T) and q_{tot} (P,T) are excess and total adsorption, respectively, ρ_{sat} is the density of the liquid gas at its boiling point and 1 bar. For reference, the ρ_{sat} values for CO_2, CH_4, CO, and H_2 at these conditions are 17.52, 26.34, 28.23, 35.12 mmol/cm^3, respectively. The gaseous density at a specific pressure and temperature (i.e., ρ_{gas} (P,T)) was gathered from the NIST database.[22] The IAST selectivities were calculated from the high-pressure adsorption isotherms using the method detailed by Wu et al.,[23] Schell et al.,[24] and S. Sircar.[25] It should be noted here that the individual partial pressures of the adsorbates (i.e., 5 % CO, 5 % CH_4, 75 % H_2 and 15 % CO_2) were considered in calculating the H_2 selectivity relative to the rest of the multicomponent mixture across the 0–50 bar pressure range.

2.3. Multicomponent breakthrough experiments

Multicomponent breakthrough experiments were performed in a lab-scale fixed-bed unit which was detailed in our previous work.[19] A 1.25 × 15 cm stainless-steel column was fully loaded with activated carbon. The height of the adsorbent bed was held constant at 15 cm for all experiments (both PSA and breakthrough), so the weight of activated carbon used for the different samples was varied to account for differences in density. To this end, the weights of AC-3, AC-6, and AC-9 used in all experiments were 6.2, 7.0, and 7.1 g, respectively. The column was equipped with an electrical heater that was controlled using a thermocouple mounted on the outer wall of the column. The temperature was recorded along the bed with different locations at four points inside of the bed in the following sequence: T_1 (L = 3 cm from bottom), T_2 (L = 6 cm from bottom), T_3 (L = 9 cm from bottom), and T_4 (L = 12 cm from bottom) and one point on the wall T_5 (bed wall), while T_6 and T_7 were the gas temperatures at the inlet and outlet of the column, respectively. The multicomponent breakthrough experimental setup is described in our previous works and was used here without modification.[19,26,27] The feed compositions considered for these experiments were 75 % H_2, 5 % CO, 5 % CH_4, and 15 % CO_2, as this composition is relatively synonymous with the feedstocks of industrial H_2 sources,[28–31] and the superficial velocity of the feedstock was held constant at 0.82 cm/s. Prior to the experiments, the samples were degassed at 200 °C for 4 h under 0.82 cm/s of He flow. The heat transfer rate at each point was calculated using the method detailed in our earlier work.[19] The concentration profiles for all species were measured using a BELMass mass spectrometer in both the breakthrough and PSA runs. The various kinetic parameters were determined from the breakthrough curves using the parameter estimation approach detailed in our earlier work.[19] The associated equations and kinematic constants are detailed in **Eqs. S1-S14** and **Table S3-S4**, respectively. The following assumptions were made in the parameter estimation: (i) the gas behaved ideally, (ii) there were no radial gradients of mass, bed porosity, gas concentration, and/or velocity along the bed, (iii) axial dispersion was sufficiently small to be neglected, (iv) constant porosity along the bed, (v) viscosity was independent of pressure, and (vi) the external and internal mass transfer resistances followed the film and linear driving force models, respectively.[30]

2.4. Pressure swing adsorption experiments

The PSA experiments were conducted using our single-column system and 4-step configuration – (i) pressurization, (ii) adsorption, (iii) depressurization, and (iv) purge – detailed in our previous work.[32] The corresponding step times are summarized in Table 1. Across all experiments, the column was first pressurized with 3.4 cm/s of H_2 at step rate of 3.5 bar/min to 34 bar. The pressure was maintained at 34 bar during the adsorption step where 3.4 cm/s of simulated SMR off-gas stream was fed until 5 % breakthrough of the feed was observed. Here, it should be noted that the time at which 5 % of the heavy component that broke through the column first (e.g., $t_{5\%}$) was collected from the breakthrough curves for each sample. These values were considered to be the optimal time for swinging the adsorption step, as this is consistent with industrial practice. After $t_{5\%}$ was reached, the column was depressurized to 1 bar at a rate of 2.04 bar/min without flowing any carrier gas. Finally, the system was purged with 3.4 cm/s of H_2 before repressurizing the system. The component purities, recoveries, and H_2 productivities were calculated from the PSA data using the equations detailed in Requfe et al.[33] and Ayub et al.,[28].

3. Results and discussion

3.1. Textural properties of the activated carbons

The N_2 physisorption isotherms and pore distributions of the activated carbons are shown in Fig. 1, and the corresponding textural properties are summarized in Table 2. From Fig. 1a, all samples displayed hybrid Type I-IV adsorption behavior with Type H4 hysteresis. Such behavior is classified by the IUPAC as coinciding with materials that are predominately microporous but contain a significant amount of mesopore volume.[34] Indeed, this hierarchal pore structure was validated by the pore distributions for the activated carbons (Fig. 1b) and is typical for activated carbon sorbents reported in various literary sources.[35,36] However, while the general pore structure was similar between the three carbons, it should be noted here that AC-6 and AC-9 had much higher surface area and pore volume compared to AC-3, which was expected to correlate to better separation performance for PSA purification of H_2. The reason being that PSA performance is generally driven by the free pore volume of the adsorbent barring any significant mass transfer effects, since the small molecular size of H_2 generally causes adsorption to be unfavorable – even at high pressure – unless cryogenic conditions are used.[29,31,37] As such, the adsorptive performance directly correlates to the free pore volume for activated carbon media. In particular, the physisorption of gases is mostly driven by the free micropore space, with small amounts of adsorption occurring within the mesopores due to better electrostatic binding between the incumbent adsorbate and the adsorbent wall at smaller diametric thresholds. For this reason, AC-9 was anticipated to outperform AC-6 for H_2 purification, since its pore volume was more allocated to the microporous regime compared to AC-6 which was more mesoporous. Granted, there are many factors which influence the PSA performance of activated carbon adsorbents for H_2 purification, especially with regards to multicomponent separation, so the expected behavior from the textural properties (i.e., AC-3 < AC-6 < AC-9) could not be definitively concluded from the textural properties alone.

Table 1
Process conditions for PSA assessment of the three activated carbon samples.

Adsorbent	Form Factor	Weight (g)	t_{press} (min)	t_{ads} (min)	$t_{depress}$ (min)	t_{purge} (min)	t_{cycle} (min)
AC-3	Granule	6.2	20.1	16.9	28.0	50.3	116.3
AC-6	Beads	7.0	18.9	18.6	31.2	59.1	127.8
AC-9	Beads	7.3	18.8	18.0	29.6	55.4	121.8

3.2. High-Pressure pure adsorption isotherms

The unary adsorption isotherms of adsorbates were collected over the activated carbon materials, as shown in Fig. 2. As can be seen, the quantity adsorbed for all gases descended in the following order across the three materials: AC-3 < AC-6 < AC-9. Such results were expected from the textural data in Table 2, as physisorption is driven by the total free volume of the adsorbent material – especially the micropore volume – and AC-9 was slightly more porous than AC-6 which was nearly twice as porous as AC-3. On the other hand, it should be noted here that the multicomponent IAST H_2 selectivity (Fig. 2e) did not coincide with the free pore volume, indicating that other factors – such as electrostatic wall interactions, multicomponent kick-out behaviors, or molecular sieving – drive the multicomponent adsorption behavior for these materials. Such differences have important implications regarding optimization of the PSA process conditions for these materials. Namely, optimizing the adsorption step time requires swinging the system pressure once the first heavy component breaks through. It should be noted that the carbons behaved similarly in this regard in that they all showed the highest affinity towards CO_2 (Fig. 2a), followed by CH_4 (Fig. 2b), followed by CO (Fig. 2c), and finally followed by H_2 (Fig. 2d). Given this behavior, it was thusly anticipated that the adsorption step time would depend on the breakthrough of the CO component, since that species was consistently the least adsorbed. This being stated, this expectation could not be fully concluded by Fig. 2, since the static behavior does not account for kinetic competitive adsorption behaviors. Instead, this was only considered to be a first approximation of which species would drive the PSA process optimization.

The total capacities of the adsorbents are listed in Table 3 along with the literature data at 25 °C and 20 bar. Overall, the AC adsorbents exhibited comparable capacities to the reported data for other materials.[23,32,38–41] Comparing across the three AC samples, AC-9 displayed the highest capacities for all gas impurities accompanying H_2 with equilibrium adsorption capacities reaching 15.1, 6.2, and 3.5 mmol/g for CO_2, CH_4, and CO, respectively, which were 11.2, 11.2, and 10.1 % higher than those of AC-6. Moreover, the adsorption capacities of CH_4 and CO were lower than that of CO_2 for all three samples, indicating these adsorbents are primarily CO_2-selective. Also as expected, the equilibrium adsorption capacity of H_2 was much lower than those for other gases, further highlighting a good H_2 purification capability for the AC samples.

To estimate the heat of adsorption (Q_{st}) of CO_2, CH_4, CO, and H_2 over AC-9, the individual gas isotherms were fitted with Sips model at multiple temperatures (25, 40, 55 °C), as shown in Fig. 2S. The Sips model was considered here on the basis of its ability to adequately fit multicomponent adsorption isotherms over heterogenous surfaces. For our isotherms, the model adequately described the experimental observations for all gases, as also evident from the high regression coefficients of up to 0.99. The fitting parameters and the corresponding correlation coefficients (R^2) are listed in **Table S2**. It should also be noted that the Q_{st} values for CO_2, CH_4, CO, and H_2 were all estimated by **Eq. S19** at constant adsorbate loading of 0.87 mmol/g, as this value was the highest H_2 capacity at 55 °C and it was reached by other gases at the same adsorption temperature. The heat of adsorption of CO_2 was found to be higher than that for CH_4 and CO, indicating that CO_2 adsorbs more strongly on AC-9 than CH_4 and CO, presumably because of stronger electrostatic adsorbate-adsorbent interactions.[7,43] Interestingly, the Q_{st} value for H_2 was estimated to be higher than for carbon-heavy gases. This contrary outcome implies that a higher adsorption heat could not always relate to a higher adsorption capacity, but rather it could mean that the adsorption capacity decreases significantly when adsorption temperature rises. Similar results were reported in literature, for example Hao et al.[44] reported that at temperatures below 353 K, the average heat of adsorption of H_2 is higher than that of CO_2 despite its lower adsorption capacity.

The kinetic H_2 purification performance of the three activated

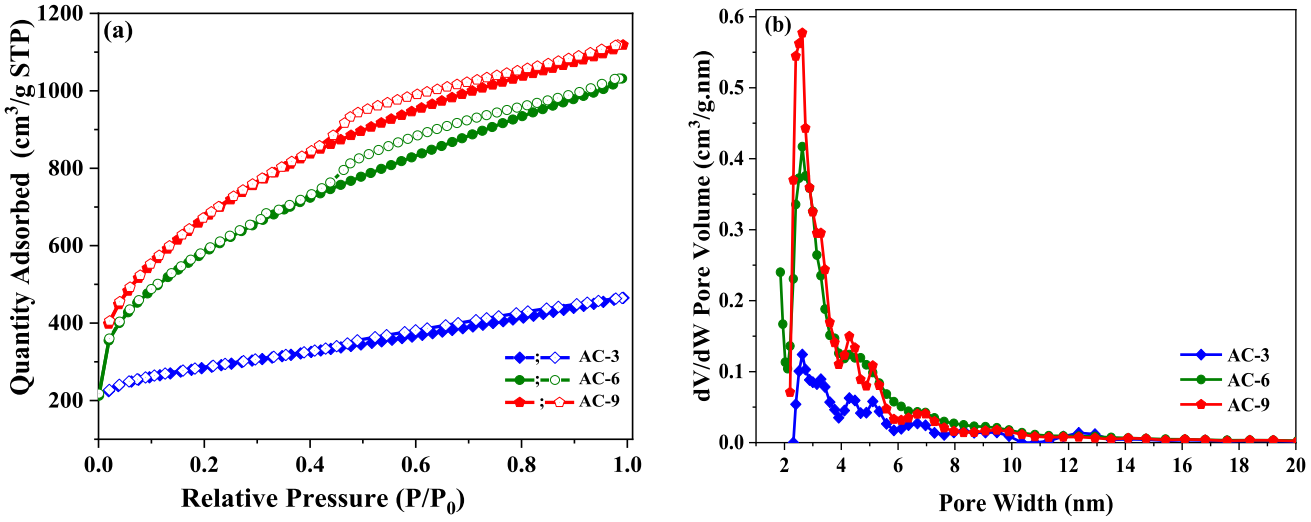

Fig. 1. (a) N_2 physisorption isotherms and (b) NLDFT pore size distribution profiles for the AC samples.

Table 2
Textural properties of the activated carbon samples.

Adsorbent	S_{BET} (m^2/g)	V_{micro} (cm^3/g)	V_{meso} (cm^3/g)	ρ_{ske} (g/cm^3)	ρ_{bulk} (g/cm^3)	d_p (nm)
AC-3	990	0.36	0.26	2.2	0.8	2.7, 3.3, 4.5, 5, 7, 12
AC-6	2140	0.65	0.96	1.9	0.5	1.9, 2.6, 4.3, 6.5, 12
AC-9	2480	0.83	0.89	1.9	0.4	2.6, 3.2, 4.3, 5, 7, 10

carbons was assessed via breakthrough tests at 34 bar and 25 °C, with desorption occurring at 1 bar. The breakthrough profiles are shown in Fig. 3 with the various constants being summarized in Table 4. The pressure drop profiles were virtually constant across the three carbons, so the pressure profiles are contained in **Figure S3, Supporting Information**. Regarding the more pertinent kinetic separation performances of the various carbons – particularly emphasizing the shapes and positions of the breakthrough profiles – it is worth noting that the order of species breakthrough corresponded perfectly with that which was shown by the adsorption isotherms in Fig. 2. Namely, the adsorbent materials had their components breakthrough in the following order: i) H_2, ii) CO, iii) CH_4, and iv) CO_2. Therefore, the PSA's adsorption step time for each material was found to be dependent on the breakthrough time for CO, given that it was the first heavy species to break through the column into the effluent stream. In particular, this led to approximate adsorbent step times of 16.9, 18.6, and 18.8 min for AC-3, 6, and 9 assuming that the time for 5 % of CO breakthrough (i.e., $t_{5\%}$) will scale linearly from 2.6 cm/s to 10.8 cm/s. For reference, $t_{5\%}$ for CO was found to be 39.8, 41.3, and 41.8 min, respectively, for AC-3, AC-6, and AC-9. This assumption can be considered reasonable based on our recent work, as it was determined that the time for breakthrough at high pressure is not influenced by molecular diffusion due to an increased driving force, instead being dependent on the feed rate of the saturating heavy species.[19] Indeed, this notion was further supported by the widths of the breakthrough fronts for each species across the various activated carbons. Namely, the breakthrough front widths (i.e., $t_{95\%}$-$t_{5\%}$) remained relatively constant across AC-3 (Fig. 3a), AC-6 (Fig. 3b), and AC-9 (Fig. 3c) regardless of which species was breaking through. Given that the front width corresponds directly to the adsorbate diffusional rate,[26] and given that the fronts were more or less parallel, it was concluded that diffusion was not the driving mechanism for adsorption within the carbonaceous adsorbents. Granted, it should be noted that the breakthrough widths for CO_2 were greater than those for the other species across all three adsorbents, which was likely caused by the materials' high affinity towards the heaviest species as was observed in Fig. 2. These findings suggest that the rate of CO_2 adsorption may be more limited by the gaseous diffusional rate compared to the other species, however, because CO_2 broke through later than the other compounds, this facet was not relevant for PSA optimization since the adsorption step time depends on the time of which heavy species is first observed. Hence, the PSA adsorption step times could be reasonably approximated by the $t_{5\%}$ breakthrough times for CO from Fig. 3.

The various breakthrough constants that were calculated from Fig. 3 are summarized in Table 4. First, it should be noted that all three carbons displayed substantially lower adsorption capacities (i.e., q at $t_{5\%}$) than would have been expected from the adsorption isotherms in Fig. 2, but the H_2 adsorption capacities were consistent with those which were observed at 34 bar in Fig. 2. Such effects do demonstrate that adsorption likely occurred in a biphasic distribution. Namely, in the first phase gaseous intrusion into the pore window was driven by the static pressure, whereas the second phase of adsorption was driven by the rate through which the heavy species diffused through the column and through the pore structure of the carbon sorbents. These trends are generally known and were to be expected from other literary sources on the subject matter.[1,32,45,46] Notably, one might expect that such reductions in adsorption capacity would not lead to significant changes in the working selectivity of the carbons, assuming that they occurred relatively constantly across the individual heavy species. However, the $(CO + CH_4 + CO_2)/H_2$ selectivities in Table 4 were all less than those observed in Fig. 2e. These changes suggest that there were differences in competing adsorption behavior during the kinetic experiments that were not anticipated from the static adsorption isotherms. In particular, the carbonaceous adsorbents captured more CH_4 than was anticipated from the adsorption isotherms. For example, AC-9 adsorbed ~ 8 mmol/g of CH_4 in Fig. 2b at $P = 34$ bar. Assuming that adsorption scales linearly with the degree of saturation, one would anticipate that 0.4 mmol/g of CH_4 should be adsorbed at 5 % saturation. However, across all three carbons the amount of CH_4 adsorbed was nearly double that value, even in AC-3 which showed significantly lower CH_4 adsorption in Fig. 2b. The increased CH_4 adsorption clearly indicates that CH_4 was more favorably adsorbed on the carbonaceous materials – at least in the initial phases of adsorption – which would reduce the number of active sites that could be saturated by the heavier components. Of course, eventually the much heavier CO_2 should kick-out the lighter CH_4, but this apparently occurred after the initial heavy species breakthrough as evidenced by the much wider fronts for CO_2 as compared to CO or CH_4. As such, it was

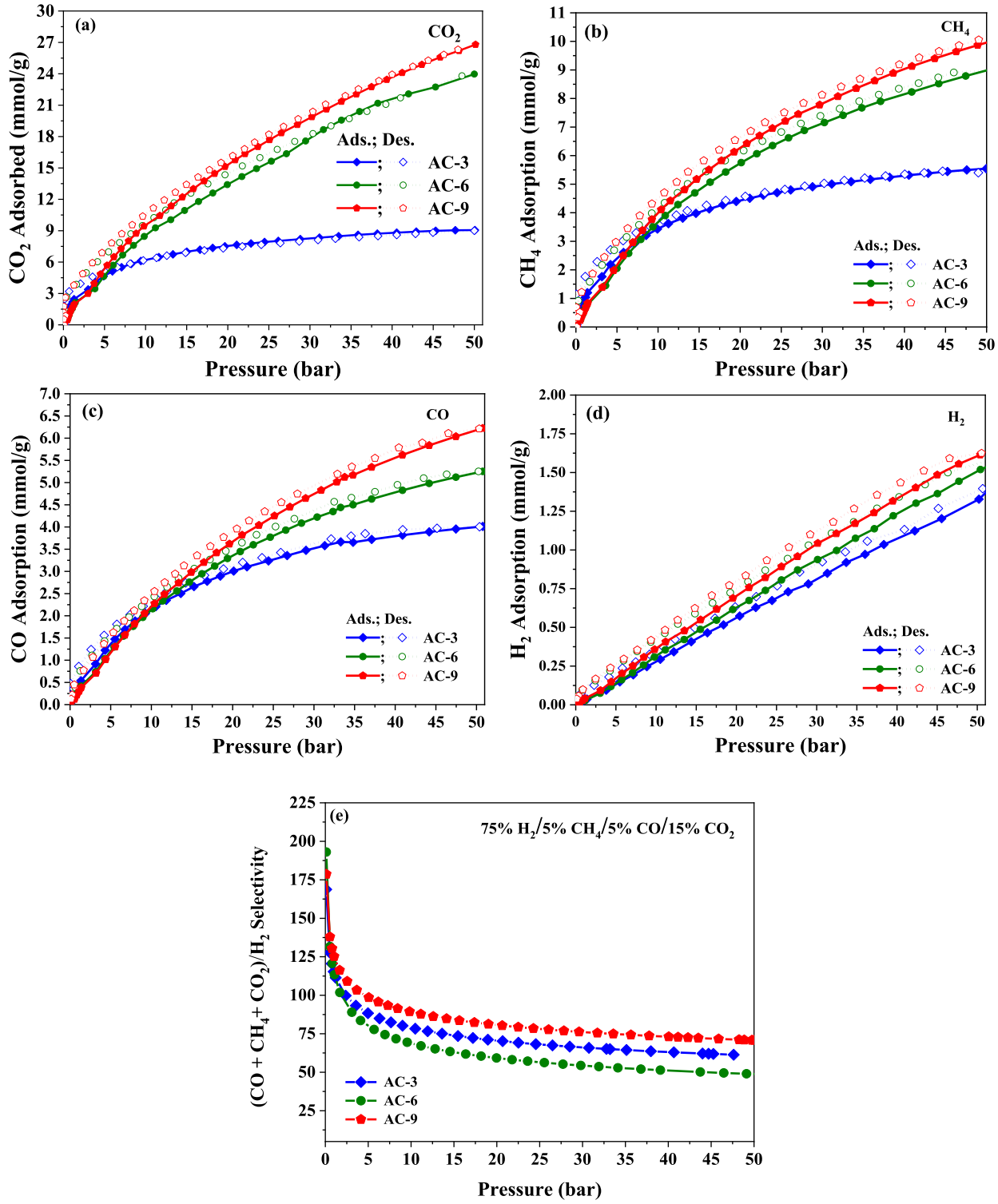

Fig. 2. High-pressure adsorption–desorption isotherms for (a) CO_2, (b) CH_4, (c) CO, and (d) H_2 from 0 to 50 bar at 25 °C, and (e) the corresponding IAST multi-component selectivities.

concluded from Table 4 that CH_4 likely adsorbs on the activated carbon materials first, thus lowering the $(CO + CH_4 + CO_2)/H_2$ selectivity.

The temperature profiles along the column length were collected during the breakthrough experiments and were used to estimate the heat transfer rate for the three commercially available activated carbons, as shown in Fig. 4. First, it should be noted here that the cycle temperature at the end of desorption was equivalent to that before adsorption, indicating that the overall net heat transfer of the process was zero. Such effects were to be expected since a true pressure swing process is considered to be thermodynamically reversible since the heat exuded during adsorption is offset by the endothermic cooling which occurs during desorption, leading to reversibility. This being stated, there were clear differences in thermodynamic properties across the different carbon materials which coincided with varying degrees of heat transfer. For

Table 3
Equilibrium capacities of CO_2, CH_4, CO, and H_2 at 25 °C and 20 bar for various adsorbents.

Adsorbent	Equilibrium capacity (mmol/g)				Ref.
	CO_2	CH_4	CO	H_2	
Zeolite 5A	6.1	4.2	4.8	0.4	[32]
Zeolite 5A-COOH	5.7	3.7	4.0	0.3	[32]
MOF-74	10.6	6.6	6.9	0.6	[32]
Zeo-A@MOF-74–1	13.1	7.7	8.0	0.9	[32]
Zeo-B@MOF-74–1	13.8	7.3	7.8	0.7	[32]
Cu-TDPAT	13.4	5.1	5.6	1.1	[23]
UTSA-16	4.6	2.3	2.5	0.3	[38]
UiO-66	6.8	3.7	2.0	–	[39]
HKUST-1	13.5	5.8	–	–	[40]
UiO-67	17.1	8.8	5.9	1.3	[41]
ZIF-8	7.5	2.8	–	0.6	[42]
AC-3	7.5	4.1	2.9	0.6	This work
AC-6	13.4	5.5	3.2	0.6	This work
AC-9	15.1	6.2	3.5	0.7	This work

instance, AC-3 (Fig. 4a), AC-6 (Fig. 4b) and AC-9 (Fig. 4c) all displayed most of their heat transfer at the inlet followed by subsequent reductions in heat transfer along the column length. Given that physisorption is an exothermic process, such behavior indicated that most of the adsorption occurred at the inlet with less adsorption occurring as the bed length increased. Indeed, the calculated heat transfer profiles along the axial length of the column (Fig. 4d) do indicate that the heat transfer decreased at higher length values. These effects are typical for granular or pellet-packed beds due to the large free volume of the adsorbent material and low surface area to volume ratio, so they were to be expected. It should be noted, however, that the calculated heat transfer also revealed that adsorption was more thermodynamically favored over AC-6 and AC-9, whose heat transfers were nearly identical, as opposed to AC-3, which had nearly double the heat transfer. The larger heat exchange from AC-3 was attributed to a higher heat of adsorption for the various species for that activated carbon owing to its lower free volume. In particular, the lower pore volume of AC-3 implied that the applied driving force to retain the adsorbates in the pore window will be higher as opposed to AC-6 or AC-9, thus leading to a greater amount of energy being transferred from adsorption. As a result, the corresponding cooling costs for AC-3 at-scale will be higher than AC-6 or AC-9, making it is less desirable for industrial applications from an energetic standpoint.

3.3. Kinetic analysis

To determine differences in dynamic separation behaviors across the three activated carbons, kinetic analysis was performed using the methodology from our previous work.[19] As shown in Fig. 5, all fittings achieved R^2 values greater than 0.99, indicating that the estimated parametric data well-represented the datasets. From these fittings, various kinetic parameters were estimated, as summarized in Table 5. As evident, the overall mass transport in all three materials was driven

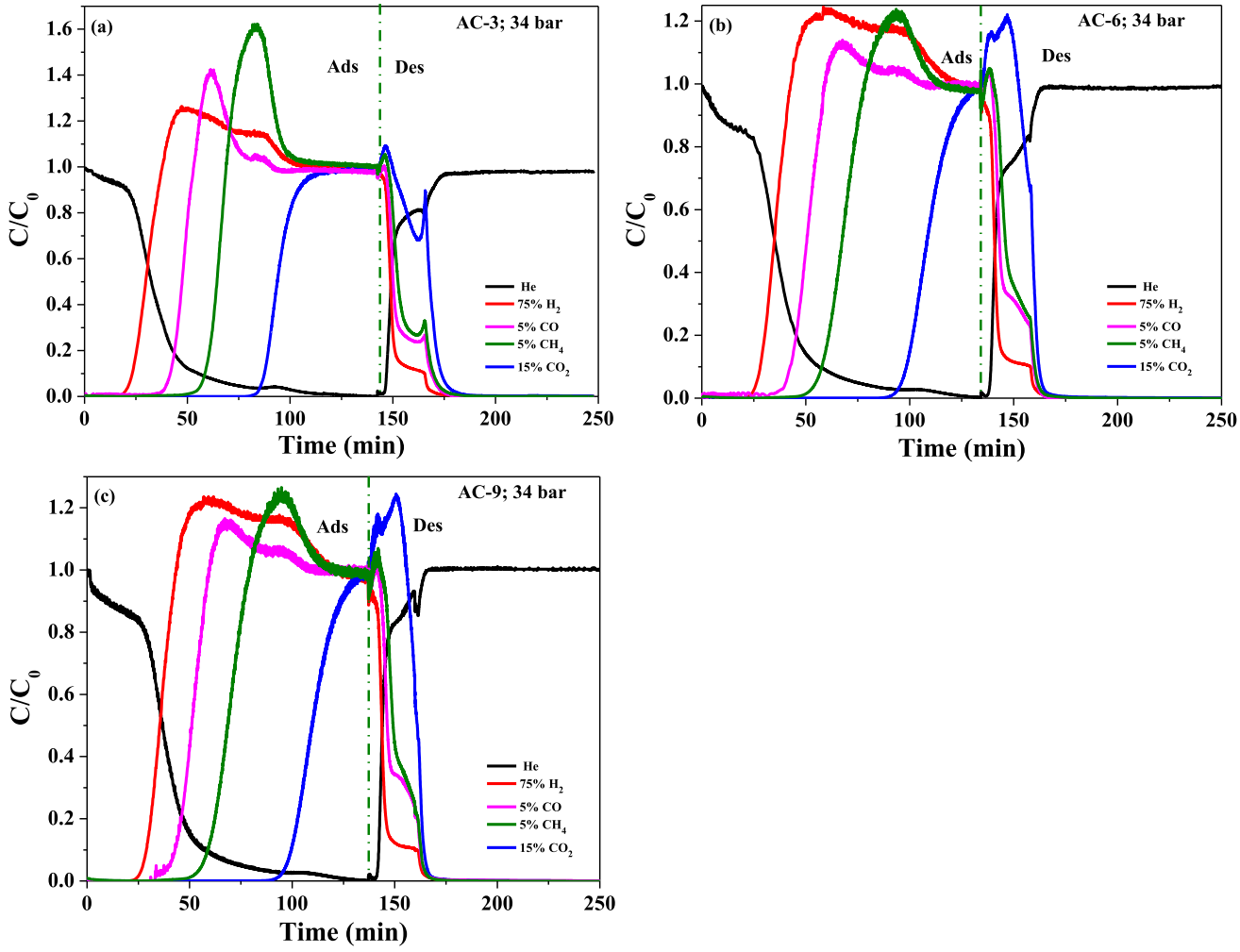

Fig. 3. Adsorption-desorption concentration profiles for multicomponent gas mixture of 75%H_2/5%CH_4/5%CO/15%CO_2 at 25 °C and (34–1) bar for (a) AC-3, (b) AC-6, and (d) AC-9 samples.

Table 4
Summary of breakthrough results for multicomponent gas mixture of 75 %H_2/5%CO/5%CH_4/15 %CO_2; feed flow rate: 2.6 cm/s, pressure: 34 bar; temperature: 25 °C.

Adsorbent	($t_{5\%}$) (min)	($t_{50\%}$) (min)	($t_{95\%}$) (min)	t_{95}-t_5 (min)	q (mmol/g)				(CO + CH_4 + CO_2)/H_2 Selectivity
					H_2 ($t_{95\%}$)	CO ($t_{5\%}$)	CH_4 ($t_{5\%}$)	CO_2 ($t_{5\%}$)	
AC-3	21.5	29.8	36.8	15.3	0.52	–	–	–	59.86
	39.8	47.7	52.5	12.7	–	0.42	–	–	
	56.5	64.4	68.4	11.9	–	–	0.71	–	
	85.8	93.9	109.1	23.3	–	–	–	4.33	
AC-6	24.9	33.9	40.9	16.0	0.68	–	–	–	52.84
	41.3	51.8	57.6	16.3	–	0.43	–	–	
	57.2	68.5	75.5	18.3	–	–	0.77	–	
	95.9	108.1	125.0	29.1	–	–	–	4.45	
AC-9	25.1	35.5	43.0	17.9	0.79	–	–	–	71.81
	41.9	52.9	58.7	16.8	–	0.45	–	–	
	57.6	68.6	77.6	20.0	–	–	0.83	–	
	96.2	109.2	126.1	29.9	–	–	–	5.21	

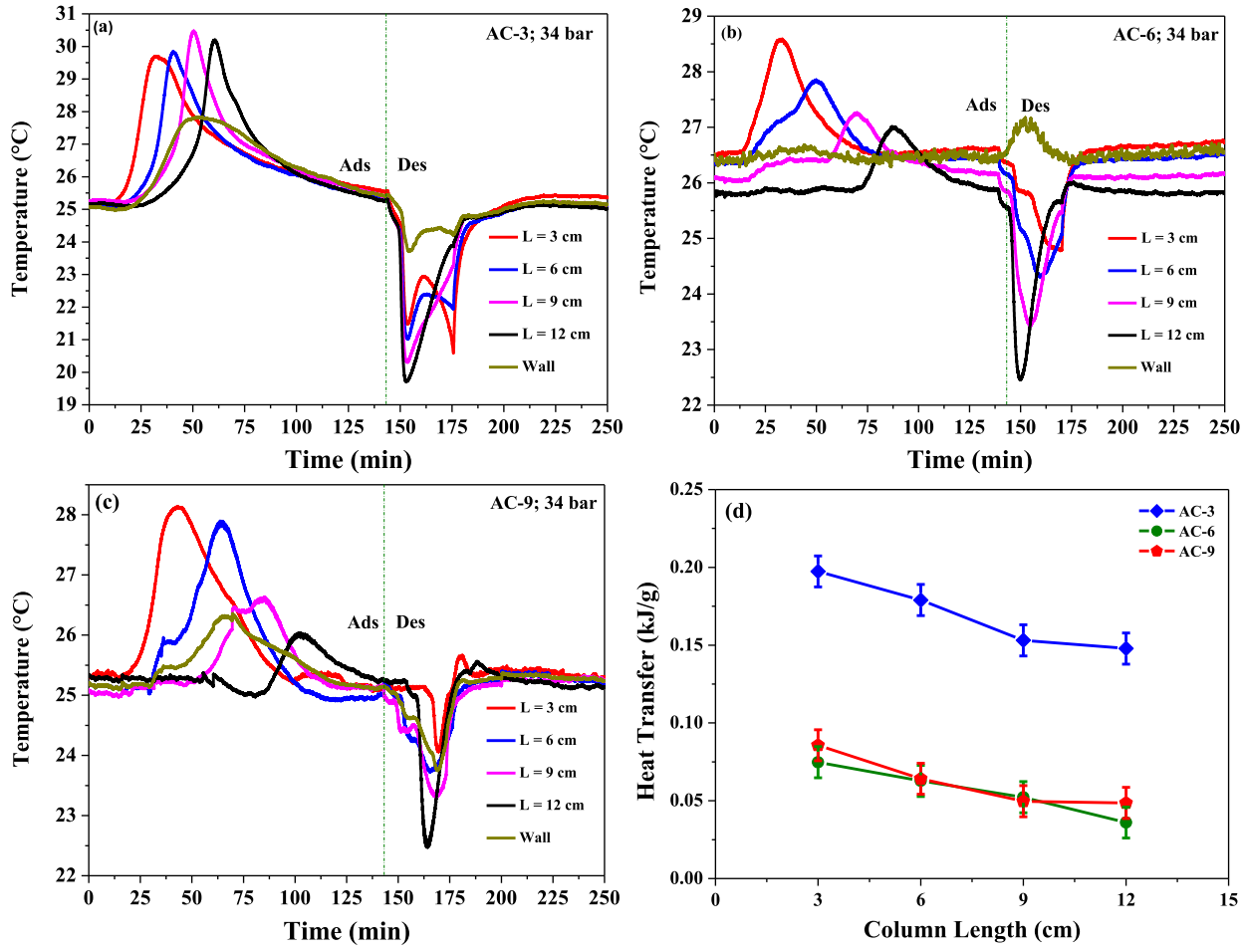

Fig. 4. Column temperature profiles from 34 bar breakthrough experiments for (a) AC-3, (b) AC-6, and (c) AC-9, and (d) the corresponding heat transfer rates as a function of column length.

primarily by the molecular transport (i.e., k_p) since it was three magnitudes larger than the film mass transport (i.e., k_f) from the bulk fluid to the surface of the adsorbents. Such behavior is well known, since the diffusion of the adsorbates through the macropores of the adsorbents is generally much slower than the film transport, the exception being when the adsorbent layer is extremely porous or sufficiently thin.[19,27,47] Given that the magnitude of k_p was much smaller than that of k_f, it was first concluded from Fig. 5 and Table 5 that the transport rates of SMR systems are primarily dependent on the rates of molecular diffusion within the walls of the carbons.

Moving onto the behaviors of the gases, which are typically discussed in terms of their effective diffusivities (i.e., D_{eff}) to account for differences in molecular diameter, the effective diffusion coefficients corresponded well with the textural properties in Table 2. Namely, the more microporous materials yielded faster effective diffusivities for all four species, leading to the effective diffusivity rates being ranked as AC-9 > AC-6 > AC-3. However, it should be noted here that, although the magnitude of the effective diffusivity was contingent on the carbon textural properties, the rankings of the individual species always followed H_2 > CO > CO_2 ≥ CH_4, indicating that the order of transport for the four gases remains constant regardless of the properties from the carbon. It should be noted here that this ranking did correspond to H_2

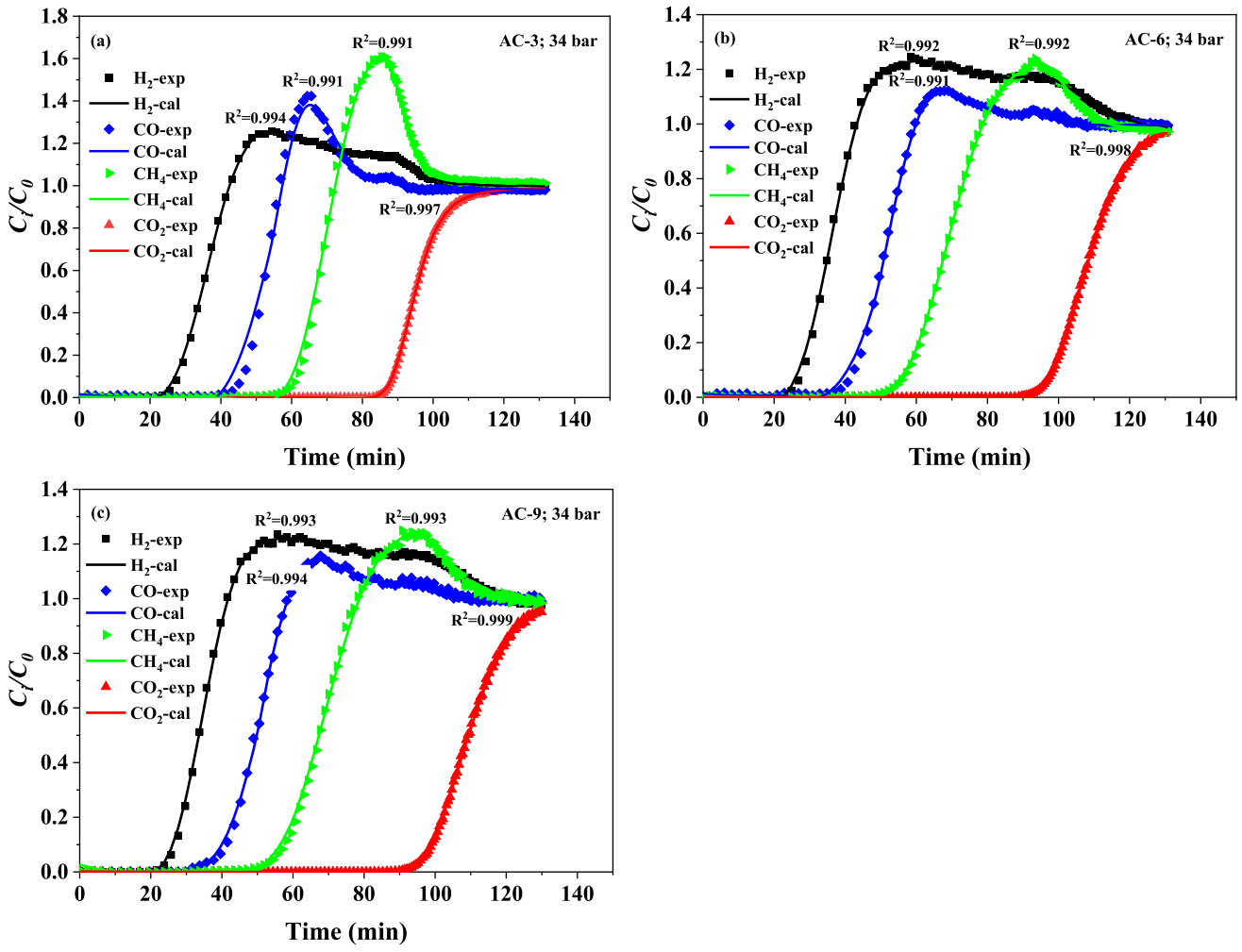

Fig. 5. Fitted breakthrough profiles for multicomponent gas mixtures of multicomponent gas mixture of 75%H_2/5%CH_4/5%CO/15%CO_2.

Table 5
Mass transfer parameters estimated from multicomponent breakthrough experiments.

Adsorbent	Gas	$k_f \times 10$ (cm/s)	$k_p \times 10^3$ (cm/s)	$D_{eff} \times 10^4$ (cm^2/s)	$k_{overall} \times 10^2$ (s^{-1})
AC-3	H_2	3.76	4.04	0.41	9.60
	CO_2	2.77	1.10	0.11	2.64
	CO	2.44	2.58	0.23	6.12
	CH_4	2.10	1.15	0.11	2.74
AC-6	H_2	1.89	9.34	1.87	10.7
	CO_2	1.39	3.80	0.77	4.44
	CO	1.22	7.09	1.42	8.04
	CH_4	1.05	3.39	0.17	3.94
AC-9	H_2	1.80	10.21	2.14	11.1
	CO_2	1.32	4.45	0.93	4.92
	CO	1.17	7.84	1.65	8.40
	CH_4	1.00	3.95	0.83	4.34

and CO breaking through as first and second, however, CH_4 consistently broke through before CO_2 even though the latter had equivalent or higher effective diffusivity. Such effects can be attributed to the heavier CO_2 kicking out the lighter CH_4 and indicated that the order at which multiple species breakthrough a column is not fully contingent on the effective diffusivity of each adsorbate. Rather, it was concluded from Fig. 5 and Table 5 that the order of breakthrough generally first depends on the rate of effective diffusivity, but the masses of the adsorbates also play a role in that heavier components can facilitate exclusion of the lighter contaminants, causing them to breakthrough earlier even though their effective diffusivity is smaller.

3.4. PSA assessment for H_2 purification

The estimated H_2 purities, recoveries, and productivities for the three activated carbons from the PSA experiments are presented in Fig. 6. As evident, the system was considered to be in steady state after cycle 4 – to the degree possible for a single column PSA system – because the fluctuations in purity/recovery/productivity were reduced to less than 1 % difference. Regarding the various performance heuristics, it should first be noted that the H_2 productivity (Fig. 6b) did not correspond with the cycle time from Table 1, but followed the order of AC-3 > AC-6 > AC-9. Instead, the throughput of AC-3 was nearly 20 % higher than that of AC-9, demonstrating that other factors aside from the total cycle time played a role in the performances of the carbons. From Fig. 6a, the driving factors seemed to be a combination of the H_2 purity and recovery. First looking at the cyclic purities, AC-3 and AC-6 had a slightly higher purity compared to AC-9, which was likely caused by the higher adsorption capacity of the latter adsorbent. The reason being that AC-9, while capable of adsorbing more of the heavy species, may not have been fully regenerated during the purge step whereas AC-3 and AC-6 were more fully regenerated. It should also be noted here that the theory of incomplete regeneration of AC-9 is further supported by the cyclic concentration profiles and temperature profiles in **Figure S4-S6**, **Supporting Information**, which showed broader desorption behavior for AC-9 (**Figure S6**) as opposed to the sharp desorption fronts observed

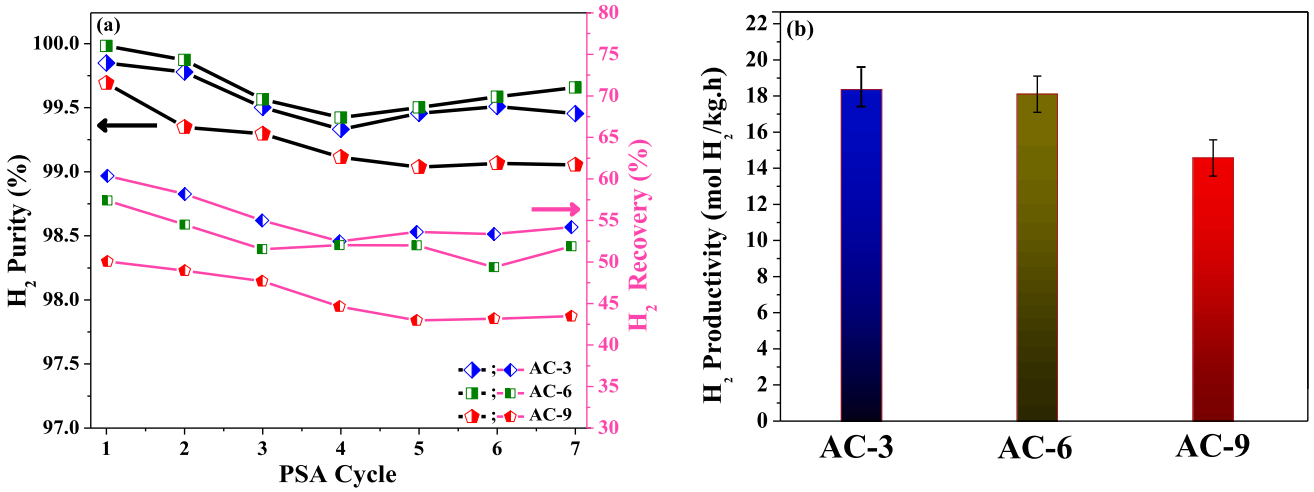

Fig. 6. (a) H_2 purity and recovery, and (b) the corresponding hourly H_2 productivity for commercially available activated carbons from PSA experiments at 25 °C.

in AC-3 (Figure S4) and AC-6 (Figure S5). Stemming from these changes, one might anticipate more heavy species hold-up in the column from AC-9 compared to AC-3 or AC-6, thus driving down the H_2 purity. Besides, the greater degree of heavy species retention also necessitated more H_2 purging, leading to an increase in light product loss by way of regenerating the column and driving down the recovery. It is likely that extending the purge time of AC-9 would lead to this sample having the best overall purity, however, such extension would further reduce the productivity of this material which was already the lowest of the three adsorbents considered. Given that all three process parameters should be balanced for overall PSA performance, such behavior indicated that high adsorbent textural properties are not necessarily the most important factor for PSA process performance. Nevertheless, extremely microporous materials – such as AC-9 – are worth using in instances where productivity is less of a factor.

It should also be noted here that AC-3 consumed more H_2 during its purge as opposed to AC-9, however, the vastly shorter cycle time and higher H_2 purity achieved by this material offset this issue, thus leading to a similar light species throughput to that of AC-6. This being the case, it should also be noted here that the H_2 recoveries and productivities for the various carbons were all higher than typically observed for systems at-scale, which typically fall within the range of 60–90 % and 2–7.2 mol/kg.h.[17,38,48,49] However, such systems contain multiple columns, whereas the system in this study is a single column system which is meant to emulate larger scale PSA processes, but should not be considered truly identical. In this context, the single-column PSA system used in this study can be used to rank various material performances within the column, but will not likely carry over to precisely the same process performance heuristics (especially recovery and productivity) in multi-column systems. Nevertheless, in the context of ranking carbons by performance, which should scale to multi-bed systems equivalently, the following carbon ranking was determined from the behavior in Fig. 6: AC-3 > AC-6 > AC-9.

The comparison of H_2 purity, productivity, and recovery over the carbon adsorbents used in this study with the available literature is provided in Table 6. Overall, comparing our experimental data with the literature data revealed a comparable H_2 purification capability for AC-3, AC-6, and AC-9 in terms of both H_2 purity and recovery. For instance, AC-3 displayed H_2 recovery of 55.3 % which was 69.8 % and 54.6 % higher than those of UTSA-16 and BPL AC, respectively. Nevertheless, the obtained H_2 recoveries over the three adsorbents were relatively lower than those reported for 5A, CaX, and layered Cu-BTC/5A, which could stem from the differences in the adsorption capacities of these adsorbents. This was mainly because the current H_2 purification process over the carbon-based adsorbents was primarily equilibrium-controlled,

Table 6
Comparison of H_2 purity, productivity, and recovery of the current study with literature.

Adsorbent	H_2 purity (%)	H_2 productivity (mol/kg.h)	H_2 recovery (%)	Ref.
BPL AC	99.9	7.20	90.0	[38]
CaX	99.7	0.24	65.0	[48]
5A	99.7	0.33	88.4	[48]
UTSA-16	99.8	1.08	16.7	[16]
C5-KS	100	3.65	57.1	[1]
CuBTC	99.9	6.80	45.7	[49]
NaX	99.9	1.57	66.3	[50]
CaX	99.9	1.84	69.6	[50]
MgX	99.9	1.56	66.2	[50]
Hollow fiber	99.2	–	88.1	[51]
Palm kernel shell AC	100	–	88.4	[52]
13X/AC	99.0	1.40	77.3	[53]
AC-3	99.6	18.30	55.3	This work
AC-6	99.7	18.10	52.6	This work
AC-9	99.3	14.60	45.8	This work

since the kinetic effects were found to be negligible (see Fig. 5), as was confirmed by the kinetic parameters in Table 5, which were all of the same order of magnitude. It should be noted here that the elemental composition and physicochemical nature of pore surface can also strongly influence the adsorption thermodynamics and kinetics of gases, however, since the three activated carbon samples possessed similar surface properties, such effects were concluded to be negligible on the superior performance of AC-3 over AC-6 and AC-9 counterparts.

4. Conclusion

In this work, we evaluated the H_2 purification performance of three highly porous carbon adsorbents by measuring unary gas adsorption isotherms at high pressure and determining the ideal selectivity values, as well as through performing multicomponent dynamic experiments and PSA runs. From seven PSA cycles, it was shown that the activated carbon adsorbents can purify H_2 to the required levels by selectively removing CO, CH_4 and CO_2, thereby reducing their concentrations in the outlet stream to 1–5 ppm, 10–20 ppm, and 1–5 ppm, respectively. Under the conditions investigated in this study, an average H_2 product purity of 99.6 %, a recovery of 55.3 %, and a productivity of 18.3 mol_{H2}/kg.h were achieved. The comparison of the performances of AC-3, AC-6 and

AC-9 in the separation of the multicomponent gas mixture of H_2/CO/CH_4/CO_2 (75/5/5/15 vol%) by PSA revealed that AC-3 gives rise to the highest H_2 productivity and recovery with 99.6 % purity, owing to its lowest H_2 equilibrium adsorption towards the other adsorbates.

CRediT authorship contribution statement

Khaled Baamran: Investigation, Formal analysis, Writing – review & editing. **Qasim Al-Naddaf:** Methodology, Investigation. **Shane Lawson:** Formal analysis, Writing – review & editing. **A. Ali Rownaghi:** Conceptualization, Validation, Formal analysis, Writing – review & editing. **Fateme Rezaei:** Conceptualization, Formal analysis, Validation, Supervision, Funding acquisition, Writing – review & editing.

Declaration of Competing Interest

The authors declare that they have no known competing financial interests or personal relationships that could have appeared to influence the work reported in this paper.

Data availability

Data will be made available on request.

Acknowledgements

The authors thank the National Science Foundation (NSF IIP-2044726) for financially supporting this project. The authors also thank Ingevity Inc. for providing the activated carbon samples.

Appendix A. Supplementary data

Supplementary data to this article can be found online at https://doi.org/10.1016/j.seppur.2022.122695.

References

[1] F.V.S. Lopes, C.A. Grande, A.E. Rodrigues, Activated carbon for hydrogen purification by pressure swing adsorption: Multicomponent breakthrough curves and PSA performance, Chem. Eng. Sci. 66 (2011) 303–317.
[2] B. He, J. Liu, Y. Zhang, S. Zhang, P. Wang, H. Xu, Comparison of structured activated carbon and traditional adsorbents for purification of H_2, Sep. Purif. Technol. 239 (2020), 116529.
[3] Y. Luo, Y. Wu, B. Li, T. Mo, Y. Li, S.-P. Feng, J. Qu, P.K. Chu, Development and application of fuel cells in the automobile industry, J. Energy Storage. 42 (2021), 103124.
[4] A. Golmakani, S. Fatemi, J. Tamnanloo, Investigating PSA, VSA, and TSA methods in SMR unit of refineries for hydrogen production with fuel cell specification, Sep. Purif. Technol. 176 (2017) 73–91.
[5] C.A. Grande, PSA technology for H2 separation, Hydrog, Sci. Eng. Mater. Process. Syst. Technol. (2016) 489–508.
[6] K. Liu, C. Song, V. Subramani, Hydrogen and syngas production and purification technologies, John Wiley & Sons, 2010.
[7] Q. Al-Naddaf, H. Thakkar, F. Rezaei, Novel zeolite-5A@MOF-74 composite adsorbents with core-shell structure for H_2 purification, ACS Appl. Mater. Interfaces. 10 (35) (2018) 29656–29666.
[8] A. Boretti, B.K. Banik, Advances in hydrogen production from natural gas reforming, Adv. Energy Sustain. Res. 2 (2021) 2100097.
[9] V.I. Agueda, J.A. Delgado, M.A. Uguina, P. Brea, A.I. Spjelkavik, R. Blom, C. Grande, Adsorption and diffusion of H_2, N_2, CO, CH_4 and CO_2 in UTSA-16 metal-organic framework extrudates, Chem. Eng. Sci. 124 (2015) 159–169.
[10] Z.R. Herm, R. Krishna, J.R. Long, CO_2/CH_4, CH_4/H_2 and CO_2/CH_4/H_2 separations at high pressures using Mg_2(dobdc), Microporous Mesoporous Mater. 151 (2012) 481–487.
[11] Y. He, S. Xiang, Z. Zhang, S. Xiong, C. Wu, W. Zhou, T. Yildirim, R. Krishna, B. Chen, A microporous metal–organic framework assembled from an aromatic tetracarboxylate for H_2 purification, J. Mater. Chem. A. 1 (2013) 2543–2551.
[12] F.V.S. Lopes, C.A. Grande, A.M. Ribeiro, E.L.G. Oliveira, J.M. Loureiro, A. E. Rodrigues, Enhancing capacity of activated carbons for hydrogen purification, Ind. Eng. Chem. Res. 48 (8) (2009) 3978–3990.
[13] M. Bastos-Neto, A. Moeller, R. Staudt, J. Böhm, R. Gläser, Dynamic bed measurements of CO adsorption on microporous adsorbents at high pressures for hydrogen purification processes, Sep. Purif. Technol. 77 (2) (2011) 251–260.
[14] S. Lawson, F. Rezaei, Effects of process parameters on CO_2/H_2 separation performance of 3D-printed MOF-74 monoliths, ACS Sustain. Chem. Eng. 9 (2021) 10902–10912, https://doi.org/10.1021/acssuschemeng.1c03443.
[15] D.D. Papadias, S. Ahmed, R. Kumar, F. Joseck, Hydrogen quality for fuel cell vehicles–A modeling study of the sensitivity of impurity content in hydrogen to the process variables in the SMR–PSA pathway, Int. J. Hydrogen Energy. 34 (15) (2009) 6021–6035.
[16] P. Brea, J.A. Delgado, V.I. Águeda, M.A. Uguina, Comparison between MOF UTSA-16 and BPL activated carbon in hydrogen purification by PSA, Chem. Eng. J. 355 (2019) 279–289.
[17] A.M. Ribeiro, C.A. Grande, F.V.S. Lopes, J.M. Loureiro, A.E. Rodrigues, A parametric study of layered bed PSA for hydrogen purification, Chem. Eng. Sci. 63 (21) (2008) 5258–5273.
[18] F.V.S. Lopes, C.A. Grande, A.M. Ribeiro, J.M. Loureiro, O. Evaggelos, V. Nikolakis, A.E. Rodrigues, Adsorption of H_2, CO_2, CH_4, CO, N_2 and H_2O in activated carbon and zeolite for hydrogen production, Sep. Sci. Technol. 44 (5) (2009) 1045–1073.
[19] S. Lawson, Q. Al-Naddaf, K. Newport, A. Rownaghi, F. Rezaei, Assessment of CO_2/CH_4 separation performance of 3D-printed carbon monoliths in pressure swing adsorption, Ind. Eng. Chem. Res. 60 (45) (2021) 16445–16456.
[20] S.-H. Jung, J.-S. Kim, Production of biochars by intermediate pyrolysis and activated carbons from oak by three activation methods using CO_2, J. Anal. Appl. Pyrolysis. 107 (2014) 116–122.
[21] Z.D. Herde, R. Dharmasena, G. Sumanasekera, J.S. Tumuluru, J. Satyavolu, Impact of hydrolysis on surface area and energy storage applications of activated carbons produced from corn fiber and soy hulls, Carbon Resour. Convers. 3 (2020) 19–28.
[22] E.W. Lemmon, Thermophysical properties of fluid systems, NIST Chem. Webb. NIST Stand. Ref. Database Number 69 (1998) 20899.
[23] H. Wu, K. Yao, Y. Zhu, B. Li, Z. Shi, R. Krishna, J. Li, Cu-TDPAT, an rht-type dual-functional metal–organic framework offering significant potential for use in H_2 and natural gas purification processes operating at high pressures, J. Phys. Chem. C. 116 (31) (2012) 16609–16618.
[24] J. Schell, N. Casas, R. Pini, M. Mazzotti, Pure and binary adsorption of CO_2, H_2, and N_2 on activated carbon, Adsorption. 18 (1) (2012) 49–65.
[25] S. Sircar, Comments on practical use of Langmuir gas adsorption isotherm model, Adsorption. 23 (1) (2017) 121–130.
[26] S. Lawson, B. Adebayo, C. Robinson, Q. Al-Naddaf, A.A. Rownaghi, F. Rezaei, A. Ali, The effects of cell density and intrinsic porosity on structural properties and adsorption kinetics in 3D-printed zeolite monoliths, Chem. Eng. Sci. 218 (2020), 115564, https://doi.org/10.1016/j.ces.2020.115564.
[27] Q. Al-Naddaf, S. Lawson, A.A. Rownaghi, F. Rezaei, Analysis of dynamic CO_2 capture over 13X zeolite monoliths in the presence of SO_x,NO_x and humidity, AIChE J. 66 (2020) e16297.
[28] K. Guan, J. Shen, G. Liu, J. Zhao, H. Zhou, W. Jin, Spray-evaporation assembled graphene oxide membranes for selective hydrogen transport, Sep. Purif. Technol. 174 (2017) 126–135.
[29] M. Balat, Possible methods for hydrogen production, Energy Sources, Part A Recover. Util. Environ. Eff. 31 (2008) 39–50.
[30] B. Parkinson, M. Tabatabaei, D.C. Upham, B. Ballinger, C. Greig, S. Smart, E. McFarland, Hydrogen production using methane: Techno-economics of decarbonizing fuels and chemicals, Int. J. Hydrogen Energy. 43 (5) (2018) 2540–2555.
[31] B. Arstad, J. Prostak, R. Blom, Continuous hydrogen production by sorption enhanced steam methane reforming (SE-SMR) in a circulating fluidized bed reactor: Sorbent to catalyst ratio dependencies, Chem. Eng. J. 189 (2012) 413–421.
[32] Q. Al-Naddaf, A.A. Rownaghi, F. Rezaei, Multicomponent adsorptive separation of CO_2, CO, CH_4, N_2, and H_2 over core-shell zeolite-5A@MOF-74 composite adsorbents, Chem. Eng. J. 384 (2020), 123251.
[33] M.J. Regufe, J. Tamajon, A.M. Ribeiro, A. Ferreira, U.-H. Lee, Y.K. Hwang, J.-S. Chang, C. Serre, J.M. Loureiro, A.E. Rodrigues, Syngas purification by porous amino-functionalized titanium terephthalate MIL-125, Energy & Fuels. 29 (7) (2015) 4654–4664.
[34] M. Thommes, K. Kaneko, A.V. Neimark, J.P. Olivier, F. Rodriguez-Reinoso, J. Rouquerol, K.S.W. Sing, Physisorption of gases, with special reference to the evaluation of surface area and pore size distribution (IUPAC Technical Report), Pure Appl. Chem. 87 (2015) 1051–1069.
[35] H.M. Far, S. Lawson, Q. Al-Naddaf, F. Rezaei, C. Sotiriou-Leventis, A.A. Rownaghi, Advanced pore characterization and adsorption of light gases over aerogel-derived activated carbon, Microporous Mesoporous Mater. 313 (2021), 110833.
[36] H. Steldinger, A. Esposito, K. Brunnengräber, J. Gläsel, B.J.M. Etzold, Activated carbon in the third dimension-3D printing of a tuned porous carbon, Adv. Sci. 6 (2019) 1901340.
[37] M.T. Anwar, X. Yan, S. Shen, N. Husnain, F. Zhu, L. Luo, J. Zhang, Enhanced durability of Pt electrocatalyst with tantalum doped titania as catalyst support, Int. J. Hydrogen Energy. 42 (52) (2017) 30750–30759.
[38] J.A. Delgado, V.I. Águeda, M.A. Uguina, J.L. Sotelo, P. Brea, C.A. Grande, Adsorption and diffusion of H_2, CO, CH_4, and CO_2 in BPL activated carbon and 13X zeolite: evaluation of performance in pressure swing adsorption hydrogen purification by simulation, Ind. Eng. Chem. Res. 53 (2014) 15414–15426.
[39] A.D. Wiersum, E. Soubeyrand-Lenoir, Q. Yang, B. Moulin, V. Guillerm, M.B. Yahia, S. Bourrelly, A. Vimont, S. Miller, C. Vagner, M. Daturi, G. Clet, C. Serre, G. Maurin, P.L. Llewellyn, An evaluation of UiO-66 for gas-based applications, Chem. Asian J. 6 (12) (2011) 3270–3280.
[40] Z. Liang, M. Marshall, A.L. Chaffee, CO_2 adsorption-based separation by metal organic framework (Cu-BTC) versus zeolite (13X), Energy & Fuels. 23 (5) (2009) 2785–2789.

[41] A.-M. Banu, D. Friedrich, S. Brandani, T. Düren, A multiscale study of MOFs as adsorbents in H_2 PSA purification, Ind. Eng. Chem. Res. 52 (29) (2013) 9946–9957.
[42] J. Hwang, H. Azzan, R. Pini, C. Petit, H_2, N_2, CO_2, and CH_4 unary adsorption isotherm measurements at low and high pressures on zeolitic imidazolate framework ZIF-8, J. Chem. Eng. Data 67 (7) (2022) 1674–1686.
[43] P. Ammendola, F. Raganati, R. Chirone, CO_2 adsorption on a fine activated carbon in a sound assisted fluidized bed: Thermodynamics and kinetics, Chem. Eng. J. 322 (2017) 302–313.
[44] P. Hao, Y. Shi, S. Li, X. Zhu, N. Cai, Adsorbent characteristic regulation and performance optimization for pressure swing adsorption via temperature elevation, Energy & Fuels. 33 (3) (2019) 1767–1773.
[45] C. Nicolella, M.C.M. van Loosdrecht, J.J. Heijnen, Mass transfer and reaction in a biofilm airlift suspension reactor, Chem. Eng. Sci. 53 (15) (1998) 2743–2753.
[46] P. Brea, J.A. Delgado, V.I. Águeda, M.A. Uguina, Modeling of breakthrough curves of N_2, CH_4, CO, CO_2 and a SMR type off-gas mixture on a fixed bed of BPL activated carbon, Sep. Purif. Technol. 179 (2017) 61–71.
[47] N.S. Wilkins, A. Rajendran, S. Farooq, Dynamic column breakthrough experiments for measurement of adsorption equilibrium and kinetics, Adsorption. 27 (3) (2021) 397–422.
[48] J.A. Delgado, V.I. Agueda, M.A. Uguina, J.L. Sotelo, P. Brea, Hydrogen recovery from off-gases with nitrogen-rich impurity by pressure swing adsorption using CaX and 5A zeolites, Adsorption. 21 (1-2) (2015) 107–123.
[49] B. Silva, I. Solomon, A.M. Ribeiro, U.-H. Lee, Y.K. Hwang, J.-S. Chang, J. M. Loureiro, A.E. Rodrigues, H_2 purification by pressure swing adsorption using CuBTC, Sep. Purif. Technol. 118 (2013) 744–756.
[50] P. Brea, J.A. Delgado, V.I. Águeda, P. Gutiérrez, M.A. Uguina, Multicomponent adsorption of H_2, CH_4, CO and CO_2 in zeolites NaX, CaX and MgX. Evaluation of performance in PSA cycles for hydrogen purification, Microporous Mesoporous Mater. 286 (2019) 187–198.
[51] R.P. Lively, N. Bessho, D.A. Bhandari, Y. Kawajiri, W.J. Koros, Thermally moderated hollow fiber sorbent modules in rapidly cycled pressure swing adsorption mode for hydrogen purification, Int. J. Hydrogen Energy. 37 (20) (2012) 15227–15240.
[52] I.K. Shamsudin, A. Abdullah, I. Idris, S. Gobi, M.R. Othman, Hydrogen purification from binary syngas by PSA with pressure equalization using microporous palm kernel shell activated carbon, Fuel. 253 (2019) 722–730.
[53] Y. Park, J.-H. Kang, D.-K. Moon, Y.S. Jo, C.-H. Lee, Parallel and series multi-bed pressure swing adsorption processes for H_2 recovery from a lean hydrogen mixture, Chem. Eng. J. 408 (2021), 127299.